energies

MDPI

Article

Design of Adaptive Fuzzy Sliding-Mode Control for High-Performance Islanded Inverter in Micro-Grid

Yan Yang [1], Yeqin Wang [1,*], Weixing Zhang [1], Zhenghao Li [1] and Rui Liang [1,2]

[1] School of Automation, Huaiyin Institute of Technology, Huaian 223003, China
[2] School of Electrical Engineering, China University of Mining and Technology, Xuzhou 221008, China
* Correspondence: wangyeqin@hyit.edu.cn; Tel.: +86-181-6875-6560

Abstract: In this paper, an adaptive fuzzy sliding-mode control (AFSMC) system is investigated for an islanded inverter to achieve a high-performance power supply. A sliding mode control (SMC) law is designed initially to obtain both the voltage tracking error and the current tracking error of the inverter involved, to realize both the output-voltage regulation and the current protection with global stability. Moreover, to deal with uncertainties in the practical inverter system without the chattering phenomenon, an adaptive fuzzy system embedded with a self-adjustive translation width is developed to replace the switch term of the SMC. In addition, the adaptation laws, derived from the Lyapunov stability theorem, adjust the AFSMC parameters online to guarantee optimal and robust performance. Furthermore, the superior control performance of the proposed AFSMC is verified by a numerical simulation in MATLAB, producing experimental results on the prototype in comparison with the conventional SMC.

Keywords: islanded inverter; robustness control; adaptive fuzzy sliding-mode control (AFSMC)

Citation: Yang, Y.; Wang, Y.; Zhang, W.; Li, Z.; Liang, R. Design of Adaptive Fuzzy Sliding-Mode Control for High-Performance Islanded Inverter in Micro-Grid. *Energies* **2022**, *15*, 9154. https://doi.org/10.3390/en15239154

Academic Editor: Mohamed Benbouzid

Received: 9 November 2022
Accepted: 29 November 2022
Published: 2 December 2022

1. Introduction

With the acceleration of the world's energy transformation, and the increasing proportion of distributed energy resources (DER) including photovoltaic, wind energy, and fuel cell, etc., [1–4], the supporting micro-grid (MG) plays an increasingly important role in the energy structure, especially in remote areas. To promote the local development and utilization of DER, some small-scale distributed generation (DG) installations are built to supply energy for local electrical appliances. In addition, different DGs can be paralleled to the point of common coupling (PCC) to construct a large-capacity islanded MG system [5–7]. Taking into account the diversity of the DER, high performance inverters are essential to ensure the proper operation of local loads and efficient utilization of DG units, which work as an electronic interface to translate direct current (DC) power from the DGs to the same alternating current (AC) power as the utility grid in terms of frequency and amplitude [8–10]. The inverters are known as islanded inverters and have the promising advantages of being clean, low carbon, and an efficient use of DER.

The islanded inverter works as a voltage source converter (VSC) with system uncertainties containing the DC voltage fluctuation in the front end, the external load disturbance in the output terminal, the parameter variation and unmodeled dynamic in the inverter, and the connection and disconnection of slave inverters in the master-slave MG [11,12]. A robust control scheme is mandatory for the local controller design to enhance the performance of the islanded inverter. The proportional-integral (PI) control framework is widely adopted in direct-current-controlled inverters [13,14] due to the simple structure, low cost, and ease of realization. Unfortunately, only in the direct current (DC) system can static error be eliminated, therefore the coordinate transformation is required. Moreover, perfect control performance cannot be guaranteed considering the nonlinear characteristics and system uncertainties. A proportional resonant (PR) control scheme [15] can realize no static

error tracking of sinusoidal command. However, it is sensitive to frequency deviation and difficult to design and implement on digital processors.

As a typical discrete and nonlinear control scheme, finite control set-model predictive control (FCS-MPC) has been extensively investigated and utilized in power electronics inverters [16–27], which directly calculates all possible switching states based on the mathematical model of the inverters and determines the optimal switching state according to a specified cost function without the requirement of the modulators. The FCS-MPC strategy presents its excellent merits in its fast dynamic response, easy implementation, and the ability to handle nonlinearity. However, considering that there is no pulse width modulation (PWM) process in the FCS-MPC scheme, and only one optimal switching state is selected in each control period, the variable switching frequency and scattered harmonic spectrum in the output are inevitable, which is a challenge for the filter design. Compared to three-phase and other multilevel inverters, the control performance will be degenerated with higher total harmonic distortion (THD) in single-phase inverters due to the less finite switching state [21]. Moreover, although the FCS-MPC allows taking multi-control objectives into account via the cost function design, proper weight configuration associated with the control performance is difficult and time-consuming. Furthermore, the cost function generally does not conform to the definition of the Lyapunov function, making it difficult to evaluate the control performance and analyze the stability of the designed control system [26,27]. Furthermore, the control performance of the FCS-MPC strategy heavily depends upon the accuracy of the model parameters. Therefore, extra disturbance observers are needed to reduce the parameter mismatches in the prediction process, especially the sliding mode-based observers [23–25,28], as these are the most widely used to improve the robustness of the system. For example, sliding mode observers (SMO) were designed for disturbance detection to enhance the robustness of the current controller against parameter uncertainties in the Micro-grid with uncertain electric vehicle energy storage systems [25]. The simulation results verify the effectiveness of the SMO-based FCS-MPC controller. With a different approach from the compensation strategy, Zhang et al. [29] applied the sliding mode control (SMC) to regulate the speed of the induction motors and constructed an SMC-MPC to improve the robust performance on parameter uncertainties and load disturbances, and the stability of the proposed SMC-MPTC was analyzed using Lyapunov stability theory. The experimental results justified the superiority in disturbance rejection ability and robustness against the variation of the motor parameters and the change in the load torque.

The nonlinear sliding mode control (SMC) is a famous alternative methodology with significant robustness characteristics against system uncertainty. Therefore, the SMC scheme with constant switching frequency has been widely applied in the control of electronic power converters [30–32], and the superior control performance of the SMC scheme for the islanded inverter has been verified by compared numerical simulations and experimental results with PI control in [11]. However, the inevitable chattering phenomenon enforced by the discontinuous sign function in the SMC law may result in poor dynamic response and sometimes even loss of system stability. Some improved control methods for the SMC have been proposed to alleviate the disadvantage of the conventional SMC [33–35]. Chang et al. [33] introduced an integral compensation for terminal sliding mode control (TSMC) to overcome the problems of steady-state error under disturbance for the DC/AC inverter; the effectiveness was verified in a laboratory prototype. However, the sign function was still contained, and the output voltages appeared to show obvious distortions with nonlinear loads. Observers of parameter perturbation and switching gain were designed to construct an adaptive sliding mode controller (ASMC) in [34], which significantly reduced the chattering caused by a larger switch gain and improved the disturbance rejection of the islanded parallel inverters. SMC-based controllers were applied to a hybrid AC/DC micro-grid in which to track the active/reactive power command in [35], and the switching law was replaced by a saturation function to avoid unexpected chattering and improve

control performance under nonlinear and unbalanced loads. Unfortunately, the control accuracy was susceptible to the chosen width of the boundary layer.

Fuzzy logic control is a popular intelligent control methodology that can mimic the reasoning processes of a human being. Furthermore, as a rule-based control strategy, it has excellent robustness because of its independence due to the precise mathematical model for the controlled plant. Concerning the nonlinear characteristics and the frequent changing of operation dynamics in the DER-based islanded inverter system, fuzzy logic has been extensively studied to handle the system with unpredictable uncertainties, which are difficult to obtain for practical applications [36–38]. Annapoorani et al. [37] proposed the fuzzy Logic-based integral controller for an isolated micro-grid to improve frequency control performance against varied operating conditions. The higher dynamic performance was validated compared with the conventional integral controller by simulation results. The fuzzy space vector pulse width modulation (FSV-PWM) technique was proposed in [38] to enhance the power quality of the inverter in the micro-grid cluster by optimizing the dq current commands using fuzzy logic theory. The simulated results adhering to all key global standards showed the effectiveness of the proposed FSV-PWM. Jiang et al. [15] presented an optimal nonlinear fuzzy controller that combines offline particle swarm optimization algorithm to adjust the parameters of the PR voltage and current controllers for the inverter in an islanded micro-grid, in which the error and the change of error were selected as the input variable of the fuzzy controller. However, for a high-order system with multiple input variables, it inevitably resulted in a complex and high computational burden control system. On the other hand, the global stability of the whole system was not proven by rigorous theoretical analysis in the aforementioned conventional fuzzy-based control system.

Today, the combination of fuzzy logic and the SMC has attracted great attention, particularly for nonlinear uncertain systems, to reduce fuzzy rules and guarantee stability by Lyapunov synthesis [39–44]. A fuzzy system was designed as the observer for the bound approximation and adjustment of the switch gain in the control system of the PV grid-connected inverter in [42], but the sign function and the chattering were still in the control effort, and the parameters of the fuzzy logic cannot be adaptive to uncertainties. Hou and Fei [43] proposed an adaptive fuzzy system to replace the sign function term to remedy the chattering. Moreover, another adaptive fuzzy system was adopted to approximate the unknown dynamics of the model to eliminate the dependence on an accurate model of the active power filter. Fang and Fei employed [44] an adaptive fuzzy system to compensate for the estimation error of the designed fuzzy neural network (FNN) observer and replaced the sign function in the backstepping law for the active power filter to remedy the chattering and suppress the current harmonics. However, both the FNN and the fuzzy system are involved, which leads to a more complex inference mechanism and control structure. For a high-performance islanded inverter system which considers certainties and is motivated by the opening literature, this study develops a simple-structure adaptive fuzzy system embedded with a translation width with a self-learning ability to estimate the switching control effort in the SMC law.

The main motivations of this study are as follows: (1) First, a total sliding mode surface is designed taking both the voltage tracking error and the current tracking error into account for the control law of a conventional SMC. Furthermore, the current command is determined according to the mathematical model and is limited in the control system to protect the power switch from damage by external faults. In addition, the inverter system states remain in the sliding motion from the initial instant without the reaching phase, ensuring global robustness by the designed SMC law. (2) In order to remedy the chattering phenomenon introduced by the switching part in conventional SMC and further enhance the robustness against the system uncertainties in inverter application, an adaptive fuzzy system embedded with the self-adjustive translation width is developed to mimic the switching law of an SMC. Moreover, the designed model-free fuzzy logic control law can efficiently compensate for the baseline model law without detailed information on

the system uncertainties. (3) The adaptation algorithm of the translation width and the parameter of the membership function are derived from the Lyapunov stability theorem. Moreover, the convergence of the sliding mode surface and the approximation errors of the parameters in the fuzzy system are proved by rigorous mathematical reasoning to guarantee the stability of the designed adaptive fuzzy sliding-mode control (AFSMC) system.

The rest of the organization of this study that follows the introduction is described below. The dynamic model of the islanded inverter is established in Section 2. The detailed design process of the proposed adaptive fuzzy sliding mode control (AFSMC) system for the islanded inverter is given in Section 3. Section 4 presents the numerical simulations and experimental verification of the designed AFSMC system compared to the conventional SMC scheme. Finally, some conclusions are summarized.

2. Dynamic Model of Islanded Inverter

The schematic diagram of an islanded inverter is depicted in Figure 1. A full-bridge inverter equipped with four power switches (T_{A+}, T_{A-}, T_{B+}, T_{B-}) is adopted to convert the direct current (DC) voltage V_{dc} from the DER to an alternating current (AC) voltage v_{AB}, which can supply a high-quality voltage v_o for the load (Z_l) through a low-pass LC filter, in which C is the filter capacitor at the DC side, L_f and C_f is the inductor and capacitor of the LC filter in the AC side, respectively. i_L, i_C, and i_o are the currents of the inductor (L_f), capacitor (C_f), and load (Z_l), respectively. v_{Lf} and v_{Cf} are the voltages of the inductor (L_f) and capacitor (C_f), respectively.

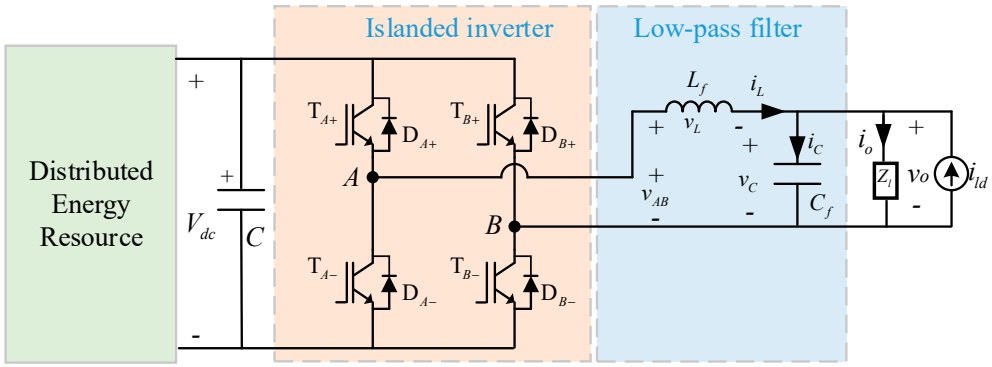

Figure 1. Schematic diagram of islanded inverter.

Generally, the interface inverters for distributed energy resources (DER) are connected to the point of common coupling (PCC) in parallel operation to expand the capacity. Figure 2 shows the structure of a parallel-inverter system in the islanded micro-grid with master-slave organization, in which an islanded inverter plays the role of master inverter to regulate the output voltage and provide the current distribution command for the slave inverter through the current sharing bus. The main objective of this paper is to develop a high-performance local voltage-mode controller for the master inverter. The local SMC-based current-mode controller for slave inverters used in the following experimental section is designed similarly to that in [11], and omitted in this paper.

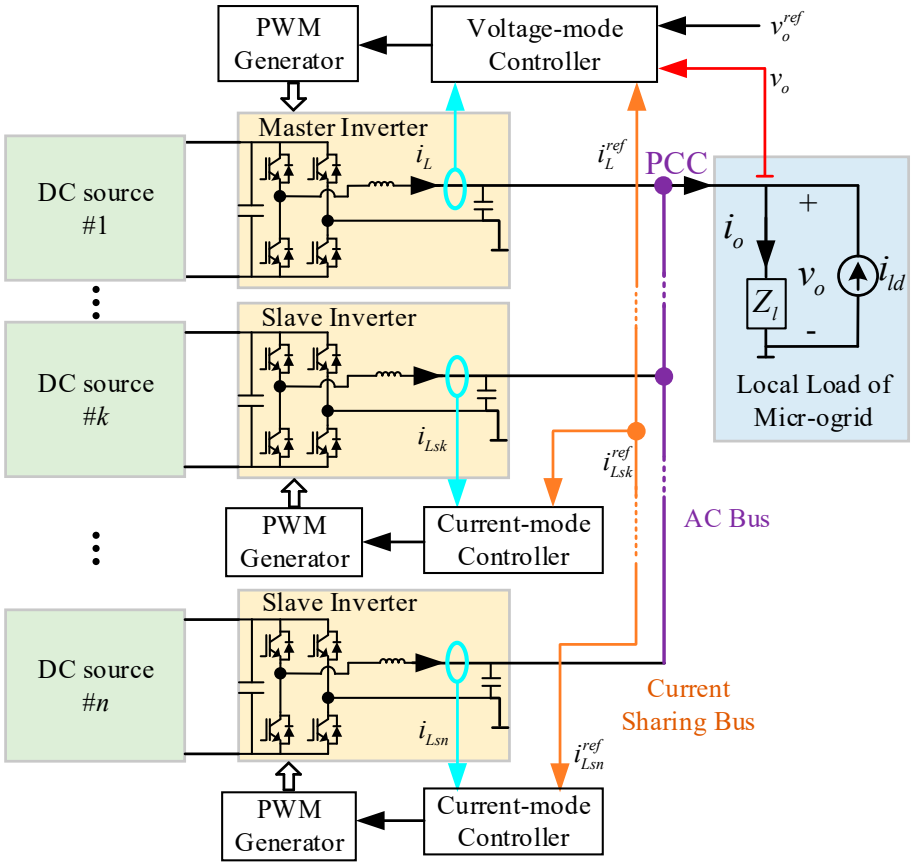

Figure 2. Structures of a parallel-inverter system in the islanded micro-grid with master-slave organization.

The average state-space method is employed to establish the average model of the master inverter, which can be represented as

$$\begin{cases} \dot{i}_L = \frac{K_{\text{PWM}}}{L_f} v_{con} - \frac{1}{L_f} v_o \\ \dot{v}_o = \frac{1}{C_f} i_L - \frac{1}{C_f} i_o \end{cases}, \tag{1}$$

where v_{con} is the control signal and is defined as the modulation signal in the unipolar PWM switching, and $K_{\text{PWM}} = V_{dc}/V_{tri}$ is the gain of the islanded inverter, in which V_{tri} is the amplitude of the selected triangular carrier signal. In practical applications, the parameters of L_f, C_f, and K_{PWM} are not the designed nominal values, thus, these parameters cannot be regarded as constants. In order to design a suitable controller to obtain a high-quality voltage for the PCC under parameter variations and external disturbance, a current source (i_{ld}) is modeled to emulate the load variations or unpredictable uncertainties.

Considering the variations of the filter parameter L_f and C_f, the fluctuation of the DC bus voltage, and the disturbance incurred by the variations in the load in the micro-grid, the mathematics model of the master inverter in (1) can be modified as follows.

$$\begin{cases} \dot{i}_L = \frac{K_{\text{PWM}n} + \Delta K_{\text{PWM}}}{L_{fn} + \Delta L_f} v_{con} - \frac{1}{L_{fn} + \Delta L_f} v_o \\ \dot{v}_o = \frac{1}{C_{fn} + \Delta C_f} i_L - \frac{1}{C_{fn} + \Delta C_f} i_o + \frac{1}{C_{fn} + \Delta C_f} i_{ld} \end{cases}, \tag{2}$$

where ΔL_f, ΔC_f, and $\Delta K_{\text{PWM}} = V_{dcn}/V_{tri}$ are the variations of L_f, C_f, and $K_{\text{PWM}} = V_{dc}/V_{tri}$, respectively.

The real state-space model for the inverter can be rearranged as two parts: (1) the nominal model of the inverter with well-known system parameters and the external

disturbance absenting; and (2) the system lumped uncertainties d_i and d_v, can be expressed as follows:

$$\begin{cases} \dot{i}_L = \frac{K_{\mathrm{PWM}n}}{L_{fn}} v_{con} - \frac{1}{L_{fn}} v_o + d_i \\ \dot{v}_o = \frac{1}{C_{fn}} i_L - \frac{1}{C_{fn}} i_o + d_v \end{cases}, \tag{3}$$

where $K_{\mathrm{PWM}n}$, L_{fn} and C_{fn} are the nominal values of K_{PWM}, L_f and C_f. Moreover, d_i and d_v are the system lumped uncertainties which can be expressed as

$$\begin{cases} d_i = \frac{\Delta K_{\mathrm{PWM}} L_{fn} - K_{\mathrm{PWM}n} \Delta L_f}{L_{fn}(L_{fn}+\Delta L_f)} v_{con} + \frac{\Delta L_f}{L_{fn}(L_{fn}+\Delta L_f)} v_o \\ d_v = \frac{-\Delta C_f}{C_{fn}(C_{fn}+\Delta C_f)} i_L + \frac{\Delta C_f}{C_{fn}(C_{fn}+\Delta C_f)} i_o + \frac{1}{C_{fn}+\Delta C_f} i_{ld} \end{cases}, \tag{4}$$

Defining the system state vector as $\boldsymbol{x} = [i_L \; v_o]^T$, the state-space model for the inverter can be represented in matrix form as

$$\dot{\boldsymbol{x}}(t) = \boldsymbol{A}_{pn}\boldsymbol{x}(t) + \boldsymbol{B}_{pn}u(t) + \boldsymbol{C}_{Pn}z(t) + \boldsymbol{d}(t), \tag{5}$$

where $u = v_{con}$ is the control input vector, $z = i_o$, and $\boldsymbol{d}(t) = [d_i \; d_v]^T$ is defined as the system lumped uncertainty, respectively; $\boldsymbol{A}_{pn} = \begin{bmatrix} 0 & -1/L_{fn} \\ 1/C_{fn} & 0 \end{bmatrix}$, $\boldsymbol{B}_{pn} = \begin{bmatrix} K_{\mathrm{PWM}n}/L_{fn} \\ 0 \end{bmatrix}$, $\boldsymbol{C}_{pn} = \begin{bmatrix} -1/C_{fn} \\ 0 \end{bmatrix}$.

Assumption 1. *The defined system lumped uncertainty in (5) is bounded, and we can assume that the boundary value can be expressed as*

$$\|\boldsymbol{d}(t)\|_1 \leq D_m, \tag{6}$$

where $\|\cdot\|_1$ is the operation of the 1-norm, and D_m is a constant with positive value.

3. AFSMC Design for an Islanded Inverter

3.1. SMC Design

The objective of the controller for the islanded inverter in this paper is to regulate both the voltage of the PCC (v_o) and the inductor current (i_L) with fast response and high robustness even under the circumstance of uncertainties. First, the desired voltage and current trace response is specified by the design of the baseline model based on the nominal model shown in (1). Subsequently, a curbing controller is designed to deal with unpredictable perturbation effects caused by load disturbance and parameter variations in a practical micro-grid. Therefore, the specified performance of the baseline model design can be guaranteed. For the above purpose, the voltage of the PCC (v_o) and the inductor current (i_L) are selected as the system state vector of $\boldsymbol{x}$, and the setpoints of v_o^{ref} and i_L^{ref} are the reference vector of $\boldsymbol{x}^{ref}$.

The tracking error vector of the inductor current and the PCC voltage is defined as

$$\boldsymbol{e} = [e_i \; e_v]^T = [i_L - i_L^{ref} \; v_o - v_o^{ref}]^T = \boldsymbol{x} - \boldsymbol{x}^{ref}, \tag{7}$$

where the voltage command signal v_o^{ref} is an independent command. In contrast, the inductor current command signal i_L^{ref} can be determined as $i_L^{ref} = C_f \frac{dv_o^{ref}}{dt} + i_o$ based on (2). In addition, a limiter is used as a current protection for the inverter against external faults.

The error dynamics of the control system can be expressed as

$$\dot{\boldsymbol{e}}(t) = \boldsymbol{A}_{pn}\boldsymbol{e}(t) + \boldsymbol{B}_{pn}u_b(t) + \boldsymbol{c}(t), \tag{8}$$

where $\boldsymbol{c}(t) = \left[(v_o^{ref}/L_{fn}) - \dot{i}_L^{ref} (i_L^{ref}/C_{fn}) - (i_o/C_{fn}) - \dot{v}_o^{ref} \right]^T$.

Based on the nominal model of the islanded inverter shown in (1), the baseline model law was designed as follows:

$$u_b(t) = -\boldsymbol{k}_b \boldsymbol{e}(t) - \boldsymbol{B}_{pn}^{+1} \boldsymbol{c}(t), \tag{9}$$

where $\boldsymbol{k}_b = [k_{bi}\ k_{bv}]$ is a designed constant parameter vector; B_{pn}^{+1} is the left pseudoinverse of B_{pn} (i.e., $B_{pn}^{+1} = (B_{pn}^T B_{pn})^{-1} B_{pn}^T$).

Substituting (9) into (8), the error dynamic in (8) can be rewritten as

$$\dot{\boldsymbol{e}}(t) - (\boldsymbol{A}_{pn} - \boldsymbol{B}_{pn}\boldsymbol{k}_b)\boldsymbol{e}(t) = \boldsymbol{0}, \tag{10}$$

The parameter vector $\boldsymbol{k}_b = [k_{bi}\ k_{bv}]$ is chosen to ensure that the characteristic polynomial of the matrix $(\boldsymbol{A}_{pn} - B_{pn}\boldsymbol{k}_b)$ is strictly Hurwitz, that is, all roots of the characteristic polynomial lie strictly in the left plane, which implies that $\lim_{t\to\infty} \boldsymbol{e}(t) = \boldsymbol{0}$. Then, the stability of the designed closed-loop system can be ensured.

Moreover, the curbing control design is an integral part of the SMC law to ensure the control performance specified by the baseline model design in (9) and to guarantee the stability of the controlled system, even with the existence of unpredictable parameter variations and external disturbances. The detailed design procedure is outlined based on the real state-space model of the inverter shown in (3).

A sling-mode surface is defined as

$$s = f(\boldsymbol{e}) - f(\boldsymbol{e}_0) - \int_0^t \frac{\partial f}{\partial \boldsymbol{e}^T} (\boldsymbol{A}_{pn} - \boldsymbol{B}_{pn}\boldsymbol{k}_b)\boldsymbol{e} d\tau, \tag{11}$$

where $\boldsymbol{e}_0$ is the initial state of $\boldsymbol{e}$. The function f is designed to satisfy the condition of $\partial f/\partial e^T = [k_{si}\ k_{sv}]$.

As (11) implies, for all $t \geq 0$, $s(t) = 0$ holds. There is no reaching phase because the initial state is designed on the sliding surface to guarantee the global sliding motion of the system. According to the model, taking the system lumped uncertainties into account, one can further modify the system error dynamic as follows:

$$\dot{\boldsymbol{e}}(t) = A_{pn}\boldsymbol{e}(t) + B_{pn}u(t) + \boldsymbol{c}(t) + \boldsymbol{d}(t), \tag{12}$$

Theorem 1. *If the islanded inverter considering system uncertainties modeled as (3) is controlled by the SMC law shown in (13), then the stability of the SMC system for the voltage tracking and the current regulating of the inverter can be ensured.*

$$u_{\mathrm{SMC}} = u_b + u_c, \tag{13}$$

where u_b is given by (9), and u_c is designed as

$$u_c = -\rho \mathrm{sgn}(s) - k_c s, \tag{14}$$

where sgn(·) expresses the sign operation, and k_c are the designed positive control parameters.

Proof of Theorem 1. By considering the positive definite Lyapunov candidate function $V_1 = s^2/2$, then, by differentiating (11) and substituting (9) and (14) into the derivative of V_1 with respect to time, it yields as follows:

$$\begin{aligned}
&\dot{V}_1 = s\dot{s} \\
&= s\tfrac{\partial f}{\partial e^T}[\boldsymbol{A}_{pn}\boldsymbol{e} + \boldsymbol{B}_{pn}(u_b + u_c) + \boldsymbol{c} + \boldsymbol{d} - (\boldsymbol{A}_{pn} - \boldsymbol{B}_{pn}\boldsymbol{k}_b)\boldsymbol{e}] \\
&= -(k_{si}K_{PWMn}/L_{fn})s\rho\mathrm{sgn}(s) - (k_{si}K_{PWMn}/L_{fn})k_c s^2 + s(k_{si}d_i + k_{sv}d_v), \\
&\le -k_s\rho|s| - k_s k_c s^2 + (k_{si}|d_i| + k_{sv}|d_v|)|s| \\
&\le -[k_s\rho - (k_{si}|d_i| + k_{sv}|d_v|)]|s| - k_c k_s s^2
\end{aligned} \tag{15}$$

where $k_s = k_{si}K_{\mathrm{PWM}}/L_f$. If the control gain ρ in (14) is chosen to satisfy the condition of $k_s\rho > (k_{si}|d_i| + k_{sv}|d_v|)$, then, (15) can be rewritten as

$$\dot{V}_1 = s\dot{s} \le -k_c k_s s^2 \le 0, \tag{16}$$

From (16), it can be concluded that $\dot{V}_1$ is a negative semidefinite function, which means that s is a bounded function, and the designed total sliding mode surface shown in (11) will converge to zero as $t \to \infty$ according to the Lyapunov stability theory and Barbalat's lemma [45]. Therefore, the sliding motion throughout the whole control process can be ensured, and the designed SMC system possesses global stability even in the circumstance of the system uncertainties. This finishes the proof of Theorem 1. □

3.2. Adaptive Fuzzy SMC (AFSMC) Design

In the SMC, the switching process generated by (14) will inevitably bring about the chattering phenomenon, which will have detrimental impacts on the control performance. To solve the above drawback of SMC and achieve a high-performance islanded inverter, in this section an adaptive fuzzy compensated scheme will be designed to imitate the SMC law shown in (13) to remedy the chattering phenomenon.

The total sliding mode surface (s) shown in (11) is chosen as the input variable of the designed fuzzy system, and the output linguistic variable is utilized to imitate the SMC law and generate the AFSMC law (u_{AFSMC}). Significantly, compared to the conventional fuzzy control with the error state of the voltage and voltage working as the input variable for the inverter system, the fuzzy combined with SMC adopted in this paper can refrain from the huge number of fuzzy rules. Afterward, the design process of the control system can be simplified and the computational burden can be lessened. The framework of the proposed adaptive fuzzy sliding mode control (AFSMC) for an islanded inverter is shown in Figure 3a.

3.2.1. Fuzzification and Membership Function

The associated antecedent fuzzy set {P, N, Z} is designed for the input linguistic variable (s). The Gaussian membership function depicted in Figure 3b is adopted in the AFSMC system and, considering the sinusoidal voltage signal, three equal parts are selected for the antecedent fuzzy sets in this paper, which can be expressed as follows:

$$w_i(s) = \exp[-(-s - m_i)^2/(c_i)^2]\Big|_{i=1,2,3}, \tag{17}$$

where $m_i|_{i=1,2,3}$ is the mean values and $c_i|_{i=1,2,3}$ is standard deviation values in the ith Gaussian function for the input, respectively. And exp(·) represents an exponential opera.

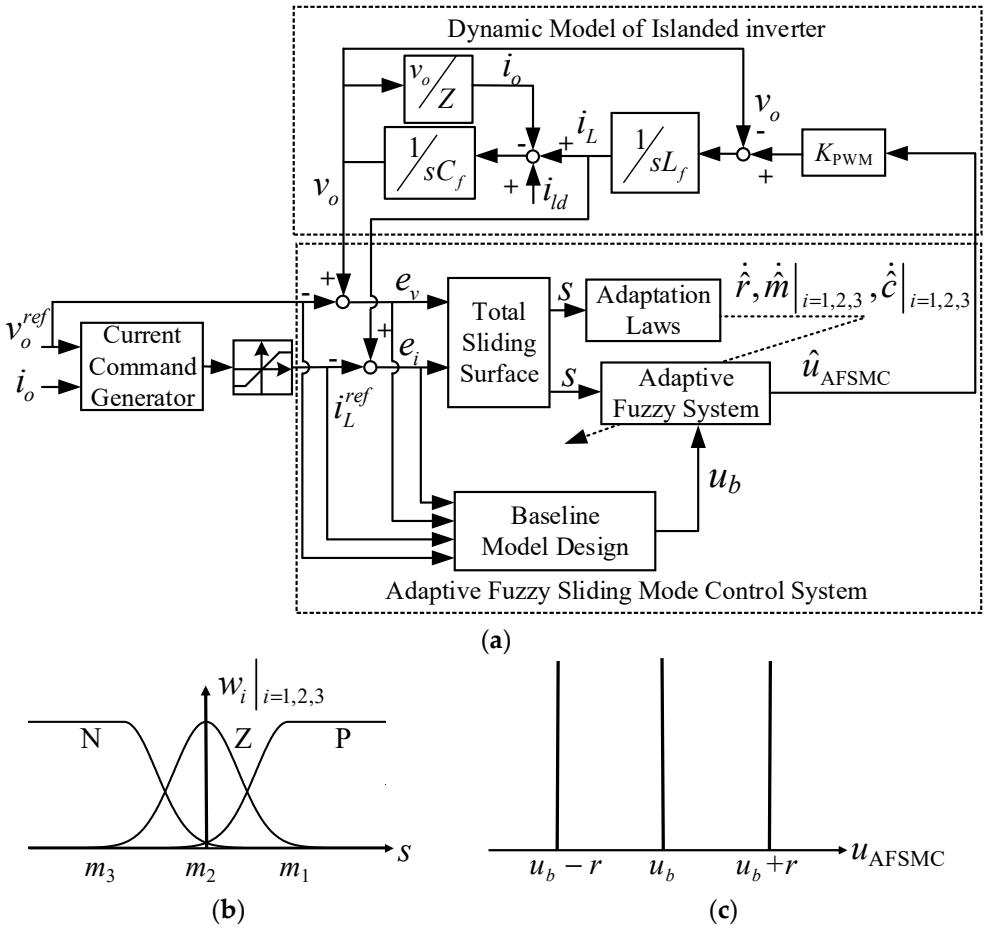

Figure 3. Proposed AFSMC system for islanded inverter: (**a**) Framework; (**b**) Membership function for input fuzzy sets of the fuzzy system; (**c**) Output fuzzy sets of the fuzzy system.

3.2.2. Fuzzy Rules and Fuzzy Reasoning

In order to avoid the unnecessary switching process, a translation width (r) is introduced to the fuzzy sliding mode (FSMC) system to imitate the curbing control effort, and to realize the following regulating process: the curbing control should vanish if the system state is near the sliding surface. While the system state takes away from the sliding surface, the curbing control should be active to force the system state trajectories toward the sliding surface rapidly and stay on it. Then, the consequent fuzzy set for the output linguistic variable u_{AFSMC} is defined as:

$$\{\mathrm{DE}, \mathrm{BL}, \mathrm{IN}\}, \tag{18}$$

The fuzzy linguistic IF-THEN rules for the designed AFSMC system can be expressed as follows:

Rule (1): If s is P, then u_{AFSMC} is DE;

Rule (2): If s is Z, then u_{AFSMC} is BL;

Rule (3): If s is N, then u_{AFSMC} is IN.

The membership function of the output linguistic variable (u_{AFSMC}) is demonstrated in Figure 3c, in which $u_b - r$, u_b, $u_b + r$ are the centers of the membership functions DE, BL, and IN, respectively.

3.2.3. Defuzzification

By the center average defuzzification method, the designed adaptive fuzzy SMC (AFSMC) can be obtained as

$$u_{\mathrm{AFSMC}} = \frac{w_1}{\sum_{i=1}^{3} w_i}(u_b - r) + \frac{w_2}{\sum_{i=1}^{3} w_i} u_b + \frac{w_3}{\sum_{i=1}^{3} w_i}(u_b + r), \tag{19}$$

3.3. Parameter Adaption Algorithm

Assumption 2. *There are optimal mean values ($m_i^*|_{i=1,2,3}$), standard deviation values ($c_i^*|_{i=1,2,3}$), and translation widths (r*) for a fuzzy controller (u^*_{AFSMC}) to approximate the SMC law (u_{SMC}) in (13). Then, the SMC law (u_{SMC}) can be rewritten as*

$$u_{\mathrm{SMC}} = u^*_{\mathrm{AFSMC}}(m_i^*|_{i=1,2,3}, c_i^*|_{i=1,2,3}, r^*) + \varepsilon_s, \tag{20}$$

where ε_s is the minimum reconstructed error vector between u^*_{AFSMC} and u_{SMC}.

The practical control law of the proposed AFSMC to approximate the SMC law (u_{SMC}) can be expressed as

$$\hat{u}_{\mathrm{AFSMC}}(t) = u_b - \hat{r}\left(\frac{\hat{w}_1}{\sum_{i=1}^{3} \hat{w}_i} - \frac{\hat{w}_3}{\sum_{i=1}^{3} \hat{w}_i}\right), \tag{21}$$

where $\hat{r}$ and $\hat{w}_i|_{i=1,2,3}$ are the estimated values of r^* and $w_i^*|_{i=1,2,3}$, respectively.

Subtract (21) from (20), the imitation error ($\widetilde{u}_s$) is written as

$$\widetilde{u}_s = u_{\mathrm{SMC}} - \hat{u}_{\mathrm{AFSMC}} = u^*_{\mathrm{AFSMC}} + \varepsilon_s - \hat{u}_{\mathrm{AFSMC}}, \tag{22}$$

For ease of stability analyses, the partially linearization of the imitation error ($\widetilde{u}_s$) by the Taylor series expansion can be represented as

$$\begin{aligned} \widetilde{\boldsymbol{u}}_s &= \left[\tfrac{\partial \hat{u}_{\mathrm{AFSMC}}}{\partial \hat{r}}|_{\hat{r}=r^*}(r^* - \hat{r}) + h_r\right] + \textstyle\sum_{i=1}^{3}\left[\tfrac{\partial \hat{u}_{\mathrm{AFSMC}}}{\partial \hat{w}_i}\big|_{\hat{w}_i=w_i{}^*}(w_i{}^* - \hat{w}_i) + h_{wi}\right] + \varepsilon_s \\ &= \left[\tfrac{\partial \hat{u}_{\mathrm{AFSMC}}}{\partial \hat{r}}|_{\hat{r}=r^*}\widetilde{r} + h_r\right] + \textstyle\sum_{i=1}^{3}\left[\tfrac{\partial \hat{u}_{\mathrm{AFSMC}}}{\partial \hat{w}_i}\big|_{\hat{w}_i=w_i{}^*}\widetilde{w}_i + h_{wi}\right] + \varepsilon_s \\ &= -w_r\widetilde{r} - \hat{r}\textstyle\sum_{i=1}^{3}(w_{gi}\widetilde{w}_i) + h_r + \sum_{i=1}^{3} h_{wi} + \varepsilon_s \\ &= -w_r\widetilde{r} - \hat{r}\textstyle\sum_{i=1}^{3}(w_{gi}\widetilde{w}_i) + v_u \end{aligned}, \tag{23}$$

where $\hat{w}_s = \sum_{i=1}^{3}\hat{w}_i$; $\widetilde{r} = r^* - \hat{r}$; $\widetilde{w}_i|_{i=1,2,3} = (w_i{}^* - \hat{w}_i)|_{i=1,2,3}$; $w_r = (\hat{w}_1 - \hat{w}_3)/\hat{w}_s$, $w_{g1} = (\hat{w}_2 + 2\hat{w}_3)/\hat{w}_s{}^2$, $w_{g2} = (\hat{w}_3 - \hat{w}_1)/\hat{w}_s{}^2$ and $w_{g3} = (-\hat{w}_2 - 2\hat{w}_1)/\hat{w}_s{}^2$; h_r and $h_{wi}|_{i=1,2,3}$ are higher order terms in Taylor series of $\widetilde{u}_s$; $v_u = h_r + \sum_{i=1}^{3} h_{wi} + \varepsilon_s$.

Moreover, the linear form of $\widetilde{w}_i|_{i=1,2,3}$ can be expressed as

$$\begin{aligned} \widetilde{w}_i &= \left[\left(\tfrac{\partial \hat{w}_i}{\partial \hat{m}_i}\big|_{\hat{m}_i=m_i{}^*}\widetilde{m}_i + h_{mi}\right) + \left(\tfrac{\partial w_i}{\partial \hat{c}_i}\big|_{\hat{c}_i=c_i{}^*}\widetilde{c}_i + h_{ci}\right)\right]|_{i=1,2,3} \\ &= (p_{mi}\widetilde{m}_i + p_{ci}\widetilde{c}_i + h_{gi})|_{i=1,2,3} \end{aligned}, \tag{24}$$

where $\widetilde{m}_i|_{i=1,2,3} = (m_i{}^* - \hat{m}_i)|_{i=1,2,3}$ and $\widetilde{c}_i|_{i=1,2,3} = (c_i{}^* - \hat{c}_i)|_{i=1,2,3}$ are the parameter approximation errors, in which $\hat{m}_i|_{i=1,2,3}$ and $\hat{c}_i|_{i=1,2,3}$ are estimated values of $m_i^*|_{i=1,2,3}$ and $c_i^*|_{i=1,2,3}$, respectively; $p_{mi} = 2\hat{w}_i\frac{s-\hat{m}_i}{\hat{c}_i{}^2}|_{i=1,2,3}$, $p_{ci} = 2\hat{w}_i\frac{(s-\hat{m}_i)^2}{\hat{c}_i{}^3}|_{i=1,2,3}$; $h_{mi}|_{i=1,2,3}$ and $h_{ci}|_{i=1,2,3}$ are higher order terms in Taylor series of $\widetilde{w}_i|_{i=1,2,3}$; $h_{gi}|_{i=1,2,3} = h_{mi} + h_{ci}$.

Then, substituting (24) into (23), the imitation error ($\widetilde{u}_s$) can be expressed in a new form:

$$\begin{aligned} \widetilde{\boldsymbol{u}}_s &= -w_r\widetilde{r} - \hat{r}\textstyle\sum_{i=1}^{3} w_{gi}(p_{mi}\widetilde{m}_i + p_{ci}\widetilde{c}_p + h_{gi}) + v_u \\ &= -w_r\widetilde{r} - \hat{r}\textstyle\sum_{i=1}^{3} w_{gi}(p_{mi}\widetilde{m}_i + p_{ci}\widetilde{c}_p) + v \end{aligned}, \tag{25}$$

where $v = \sum_{i-1}^{3} h_{gi} + v_u$.

Theorem 2. *If the fuzzy parameters of the proposed AFSMC law designed as (21) self-adjust online with the corresponding adaptation laws in (26), the convergence of the fuzzy parameters as well as the global stability of the tracking error of the inverter system in (3) can be guaranteed.*

$$\begin{cases} \dot{\hat{r}} = \eta_r s w_r \\ \dot{\hat{m}}_i|_{i=1,2,3} = \eta_{mi} s \hat{r} w_{gi} p_{mi}|_{i=1,2,3} \\ \dot{\hat{c}}_i|_{i=1,2,3} = \eta_{ci} s \hat{r} w_{gi} p_{ci}|_{i=1,2,3} \end{cases}, \tag{26}$$

where η_r, $\eta_{mi}|_{i=1,2,3}$, *and* $\eta_{ci}|_{i=1,2,3}$ *are positive learning rates.*

Proof of Theorem 2. A Lyapunov function associated with s, $\widetilde{r}$, $\widetilde{m}_i|_{i=1,2,3}$ and $\widetilde{c}_i|_{i=1,2,3}$ is defined as:

$$V_{AFSMC}(s, \widetilde{r}, \widetilde{m}_i|_{i=1,2,3}, \widetilde{c}_i|_{i=1,2,3}) = \frac{1}{2}s^2 + \frac{\widetilde{r}^2}{2\eta_w} + \frac{\sum_{i=1}^{3} \widetilde{m}_i{}^2}{2\eta_{mi}} + \frac{\sum_{i=1}^{3} \widetilde{c}_i{}^2}{2\eta_{ci}}, \tag{27}$$

By substituting (13) and (25) into (22), the practical control effort of the designed AFSMC law is rewritten as

$$\begin{array}{l} \hat{u}_{AFSMC} = u_{SMC} - \widetilde{u}_s \\ = [-\boldsymbol{k}_b \boldsymbol{e}(t) - \boldsymbol{B}_{pn}^{+1} \boldsymbol{c}(t) - k_c s - \rho(t) b_{pn}^{-1} \mathrm{sgn}(s)] \\ + w_r \widetilde{r} + \hat{r} \sum_{i=1}^{3} w_{gi} (p_{mi} \widetilde{m}_i + p_{ci} \widetilde{c}_i) + v \end{array}, \tag{28}$$

By substituting $\hat{\boldsymbol{u}}_{\mathrm{AFSMC}}$ in (28), the sliding mode surface in (11), and the adaptation laws for the fuzzy parameters in (26) into the derivative of (28), it produces the following result.

$$\begin{array}{l} \dot{V}_{AFSMC}(s, \widetilde{r}, \widetilde{m}_i|_{i=1,2,3}, \widetilde{c}_i|_{i=1,2,3}) = s\dot{s} - \frac{\widetilde{r}\dot{\hat{r}}}{\eta_r} - \frac{\sum_{i=1}^{3} \widetilde{m}_i \dot{\hat{m}}_i}{\eta_{mi}} - \frac{\sum_{i=1}^{3} \widetilde{c}_i \dot{\hat{c}}_i}{\eta_{ci}} \\ = s[-k_s \rho \mathrm{sgn}(s) - k_s k_c s + (k_{si} d_i + k_{sv} d_v)] \\ + [-w_r \widetilde{r} - \hat{r} \sum_{i=1}^{3} w_{gi} (p_{mi} \widetilde{m}_i + p_{ci} \widetilde{c}_i) + v]\} \\ - \frac{\widetilde{r}\dot{\hat{r}}}{\eta_r} - \frac{\sum_{i=1}^{3} \widetilde{m}_i \dot{\hat{m}}_i}{\eta_{mi}} - \frac{\sum_{i=1}^{3} \widetilde{c}_i \dot{\hat{c}}_i}{\eta_{ci}} \\ = s[-k_s \rho \mathrm{sgn}(s) - k_s k_c s + v_t] + V_r + \sum_{i=1}^{3} V_{mi} + \sum_{i=1}^{3} V_{ci} \\ \leq -k_s(\rho - |v_t|)|s| - k_s k_c s^2 \\ \leq -k_s k_c s^2 \leq 0 \end{array}, \tag{29}$$

where $V_r = s w_r \widetilde{r} - \widetilde{r}\dot{\hat{r}}/\eta_r$, $V_{mi} = s \hat{r} w_{mi} p_{mi} \widetilde{m}_i - \widetilde{m}_i \dot{\hat{m}}_i / \eta_{mi}$ and $V_{ci} = s \hat{r} w_{ci} p_{ci} \widetilde{c}_i - \widetilde{c}_i \dot{\hat{c}}_i / \eta_{ci}$ $v_t = v + (k_{si} d_i + k_{sv} d_v)$. One can conclude that if the condition $\rho > |v_t|$. holds, the result of $\dot{V}_{AFSMC}(s, r, \widetilde{m}, \widetilde{c}) \leq 0$ can be ensured, i.e., $V_{\mathrm{SFNNISMC}}(s(t), \widetilde{r}(t), \widetilde{m}_i(t)|_{i=1,2,3}, \widetilde{c}_i(t)|_{i=1,2,3})$ $\leq V_{\mathrm{SFNNISMC}}(s(0), \widetilde{r}(0), \widetilde{m}_i(0)|_{i=1,2,3}, \widetilde{c}_i(0)|_{i=1,2,3})$, which implies that s, $\widetilde{r}$, $\widetilde{m}_i|_{i=1,2,3}$ and $\widetilde{c}_i|_{i=1,2,3}$ are bounded, moreover, they will tend to zero as $t \to \infty$, according to Barbalat's Lemma [45]. Thus, both the convergence of the parameter adaptation for fuzzy logic and the global stability of the proposed AFSMC system can be ensured. This finishes the proof of Theorem 2. □

4. Numerical Simulations and Experimental Examination

The superiority of the proposed adaptive fuzzy sliding mode control (AFSMC) system for the islanded inverter is demonstrated by the comparative simulation and experimentation. The detailed parameters of the inverter circuit and the testing loads are described in Table 1.

Table 1. Parameters of inverter circuit and testing loads.

Circuit Parameters of Islanded Inverter	Value
DC bus voltage	400 V
AC output voltage (RMS)	220 V
Inductance of LC filter	2 mH
Capacitance of LC filter	20 μF
Fundamental Frequency	50 Hz
Switching Frequency	15 kHz
Linear resistance Load	50 Ω
Nonlinear RCD Load	50 Ω/1100 μF/KBPC3506P

To obtain the best transient control performance under the requirement of stability, the value of $\boldsymbol{k}_b = \begin{bmatrix} 3.15 \times 10^4 & 1.2 \times 10^2 \end{bmatrix}$ in (9) is selected to guarantee the designed control system to be stable, making the eigenvalues of the matrix $(\boldsymbol{A}_{pn} - \boldsymbol{B}_{pn}\boldsymbol{k}_b)$ in (10) to be on the left half plane under the nominal model. Furthermore, referring to the total sliding mode surface in (11), the parameters $k_{si} = 5.7 \times 10^3$ and $k_{sv} = 3.5 \times 10^3$ are decided to rate the level of the function $f(\boldsymbol{e})$. Additionally, the switch gain ($\rho = 1.5$) is determined by the bound of system uncertainties, and the value of $k_c = 5.5 \times 10^3$ in (14) is selected to guarantee the stability of the system even under the circumstance of the worst case circumstance $k_s\rho < (k_{si}|d_i| + k_{sv}|d_v|)$.

The sliding mode surface (s) designed as (11) is selected as the input variable of the fuzzy system. For the lowest computation burden in practical application, three equal parts fuzzy set are selected: P (positive, $i = 1$), Z (zero, $i = 2$), and N (negative, $i = 3$). Furthermore, to achieve better transient performance, the initial mean and standard deviation values of the Gaussian functions are often roughly chosen by heuristics or expert knowledge, which can be set by diving equally as $m_1 = 9$, $m_2 = 0$, and $m_3 = -9$; $c_1 = c_2 = c_3 = 9$. Furthermore, the initial translation width is simply selected as $r = 0$. Parameters will be adjusted online by the designed adaption algorithm according to the dynamic input to counter the adverse effects of the inaccurate selection of initial values. Moreover, the learning rates of the parameters are chosen as $\eta_r = 0.531$, $\eta_m|_{i=1,2,3} = \eta_c|_{i=1,2,3} = 5.05$.

The mean square error (MSE) value of the voltage tracking is defined as follows to demonstrate the control performance:

$$\mathrm{MSE}(e_v) = \frac{1}{V_{om}T}\sum_{n=1}^{T} {e_v}^2(n), \tag{30}$$

where V_{om} is the maximum value of the output voltage v_o, T is the total sampling time.

4.1. Numerical Simulations

Based on the inverter in Figure 1 and the system parameters in Table 1, the numerical simulation model is built with MATLAB software (Version 2020b). Simulations of the inverter system with the SMC law in (13) are compared to the results of the proposed AFSMC law in (21) with the adaption algorithm in (26) to evaluate the effectiveness of the improvement in tracking accuracy and the elimination of the chattering phenomenon. Moreover, the trained procedure for the parameter adaptations in the fuzzy controller is presented to exhibit the self-learning ability of the proposed AFSMC system.

In order to verify the robustness of the voltage tracking control, the system uncertainties appear at the worst case, e.g., the valley of the output voltage ($t = 0.155$) and four simulated conditions are carried out in this section: (1) The islanded inverter operates with ($R_l = 25\ \Omega$, $V_{dc} = 400$ V, $L_f = 2$ mH) at the beginning, and the external load disturbance happens with the load R_l changing from 25 Ω to 50 Ω; (2) Considering the characteristics of the distributed energy resources (DER), the DC voltage fluctuates from the nominal value of 400 V to 380 V; (3) The filter inductance variation from the nominal value of 2 mH to 1.8 mH is designed; (4) A salve inverter connects to and disconnects from the islanded inverter in a practical islanded MG application with the master-slave organization.

The numerical simulations with the SMC law and the proposed AFSMC law under the external load disturbance are depicted in Figure 4. As one can see from the results, both control methods have robust voltage-tracking performance against external load disturbance. However, it is obvious that the tracking performance will degenerate with a larger tracking error when the load changes from the nominal value of 25 Ω to 50 Ω, seen in Figure 4b, for the model-based control method of the SMC strategy. On the other hand, a larger switching gain (ρ = 10.5) chosen in Figure 4c can effectively reduce the tracking error with the MSE value reduced from 0.8774 to 0.5163. However, by observing the tracking error in Figure 4b and the control effort in Figure 4d, the severe chattering phenomenon follows, caused by the switching function in (13). Thus, the appropriate switch gain should be designed carefully according to the bounds of possible system uncertainty to ensure control accuracy and avoid increasing the chattering phenomenon. Unfortunately, it is hard to accurately inform the bounds of the system uncertainty in practical applications. On the contrary, the favorable tracking response with the MSE value of 0.2337 is obtained under the occurrence of the external load disturbance without the chattering phenomenon in the tracking error and the control effort of the proposed model-free AFSMC scheme due to the ability of the fuzzy logic to deal with the unknown process and the self-learning mechanism to adjust the control parameters online according to the instant input status.

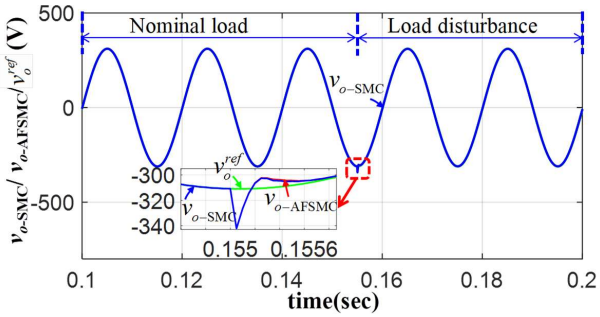

(**a**)

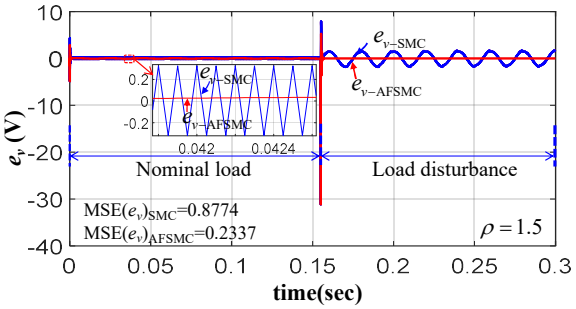

(**b**)

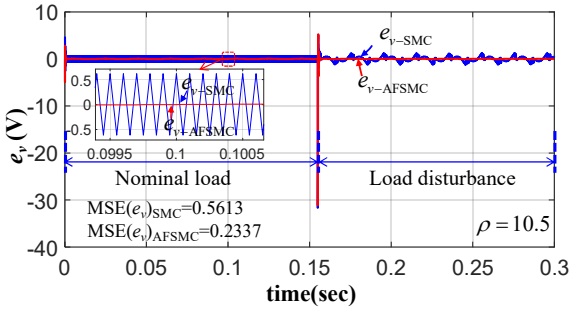

(**c**)

Figure 4. *Cont.*

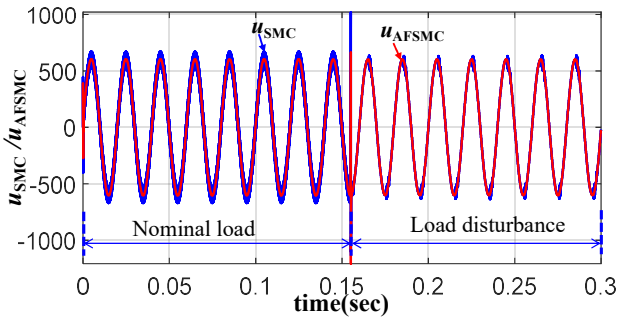

(**d**)

Figure 4. Simulated result under load disturbance from 25 Ω to 50 Ω: (**a**) Output voltage (v_o); (**b**) voltage tracking error by SMC (ρ = 1.5) and proposed AFSMC; (**c**) voltage tracking error by SMC (ρ = 10.5) and proposed AFSMC; (**d**) control effort by SMC (ρ = 10.5) and proposed AFSMC.

Taking the load disturbance, for instance, the self-learning process of the parameters in fuzzy logic associated with the load disturbance is depicted in Figure 5. Figure 5a,b shows that the mean values and the standard deviation values of the Gaussian membership functions can be adjusted online to cope with the system uncertainty. Moreover, one can see from Figure 5c, the translation width (r) is zero in the steady state, which means that the curbing control effort is not working. When the load disturbance occurs, the translation width can be tuned adaptively to an optimal value which can force the system state to hit the sliding-mode surface rapidly, and the chattering phenomenon are remedied in the control efforts at the same time. Therefore, the drawback of the conservative selection of the fixed translation width can be overcome and the satisfactory tracking performance can be obtained even under the occurrence of load disturbance, which can demonstrate that the proposed AFSMC strategy has good self-adaptability and robustness.

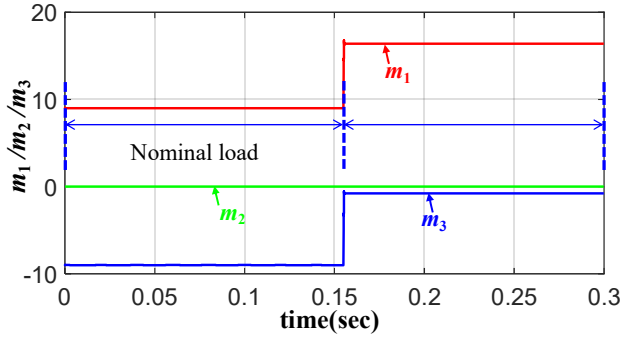

(**a**)

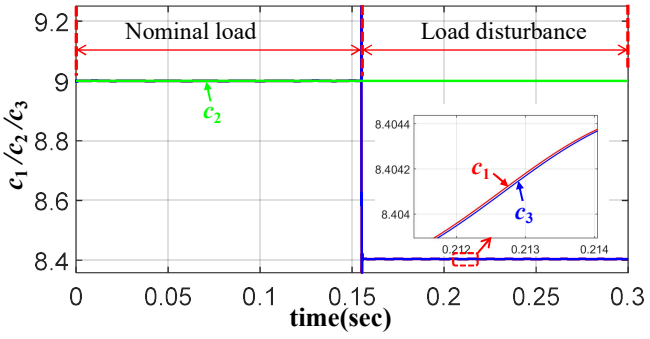

(**b**)

Figure 5. *Cont.*

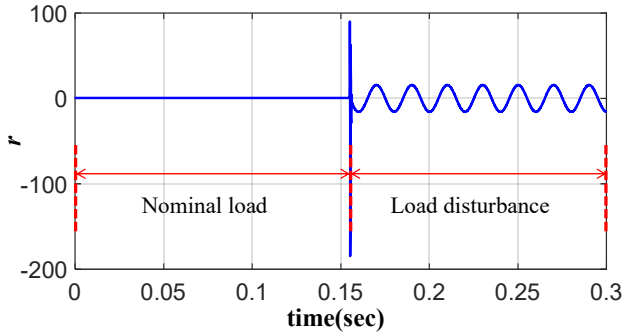

(**c**)

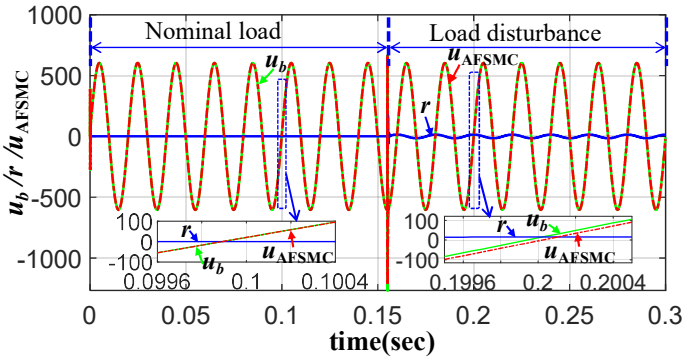

(**d**)

Figure 5. Self-learning process under load disturbance: (**a**) Mean adaption ($\widetilde{m}_i|_{i=1,2,3}$); (**b**) Standard adaption ($\widetilde{c}_i|_{i=1,2,3}$); (**c**) translation width adaption (r); (**d**) Control efforts (u_b, u_r, u_{AFSMC}).

In order to further evaluate the robustness against the system uncertainties and the effectiveness of remedying the chattering phenomenon of the proposed AFSMC scheme, the simulation of the inverter under the system uncertainties caused by the DC voltage fluctuates from the nominal value of 400 V to 380 V, and the filter-inductance varies from the nominal value of 2 mH to 1.8 mH. The associated simulation results are exhibited in Figures 6 and 7, respectively. As demonstrated by Figures 6 and 7, there are 86.4% and 68.4% improvements with the proposed AFSMC in the MSE values under the occurrence of the fluctuation DC voltage and the variation of the filter-inductance at t = 0.155 (the effects of the system uncertainties are worst at this peak and trough point), respectively. Moreover, compared to the voltage tracking error, the chattering phenomenon are effectively remedied by the online adaptation of the parameters. The control error introduced by the system uncertainties in the model-based u_b can be compensated appropriately by the model-free fuzzy controller r which takes the place of the sing function in the curbing control in (12). This demonstrates that the proposed AFSMC scheme has a superior robustness to that of the SMC scheme without chattering phenomenon. It is worth noticing that the self-learning process of the parameters under those system uncertainties is similar to the process shown in Figure 5. The associated simulated results are omitted here.

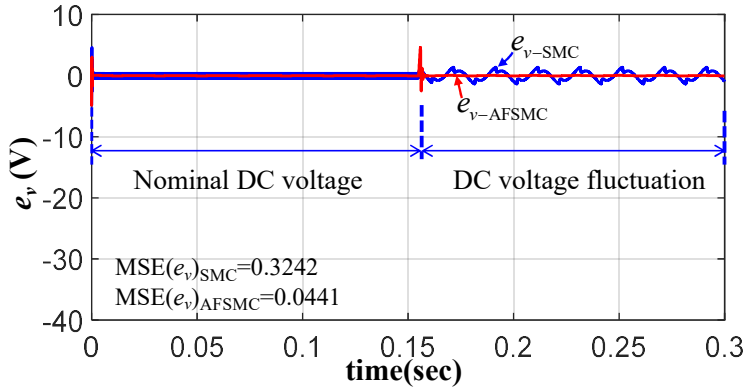

Figure 6. Simulated result of voltage tracking errors under DC voltage fluctuation from 400 V to 380 V.

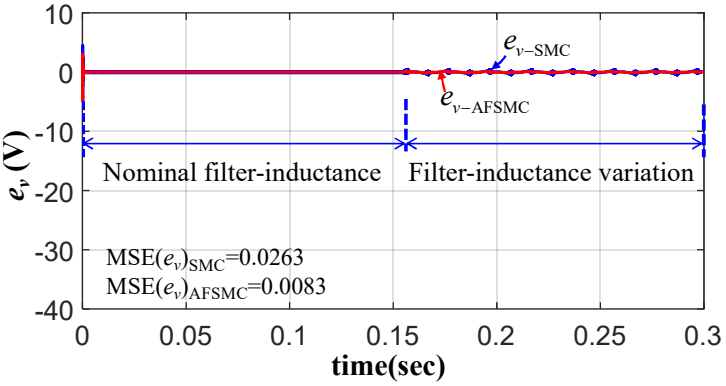

Figure 7. Simulated result of voltage tracking errors under filter-inductance variation from the nominal value of 2 mH to 1.8 mH.

In this section, the control performance of the islanded inverter as the master inverter with a slave inverter is investigated. The master inverter is responsible for the PCC voltage regulated by the SMC and the proposed AFSMC system. The slave inverter performs the current mode SMC designed in [11] to realize the current sharing with the islanded inverter. The simulations of the parallel system under the connection and disconnection of the slave inverter are shown in Figure 8. The output voltage and the voltage tracking errors are shown in Figure 8a–c; the associated currents of the master and inverter are shown in Figure 8 d,e.

As seen from the simulated results of Figure 8b,c, the parallel inverter system can maintain its stability and offer voltage sustaining when the salve inverter is connected to or disconnected from the PCC at t = 1.55 s, controlled both by the voltage controller of the SMC and the proposed AFSMC. However, the voltage track performance is significantly improved with lower MSE values (0.2835 and 0.4563) with the proposed AFSMC compared to the values (0.3787 and 0.7872) with the SMC. Moreover, the chattering phenomenon in the SMC tracking errors are remedied by the proposed AFSMC. In addition, by observing the simulated results of Figure 8d,e, the current is supplied by the master inverter when only the master inverter operates, and the current sharing is realized between the master and the slave inverter without any chattering by the proposed AFSMC under the connection of the slave inverter. The superior robustness of the proposed AFSMC with higher tracking accuracy without chattering phenomenon can also be demonstrated by the simulated results of the structure uncertainties of the islanded inverter.

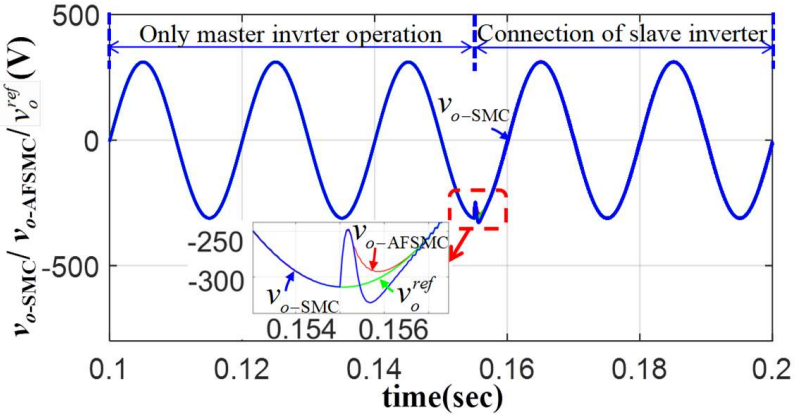

(a)

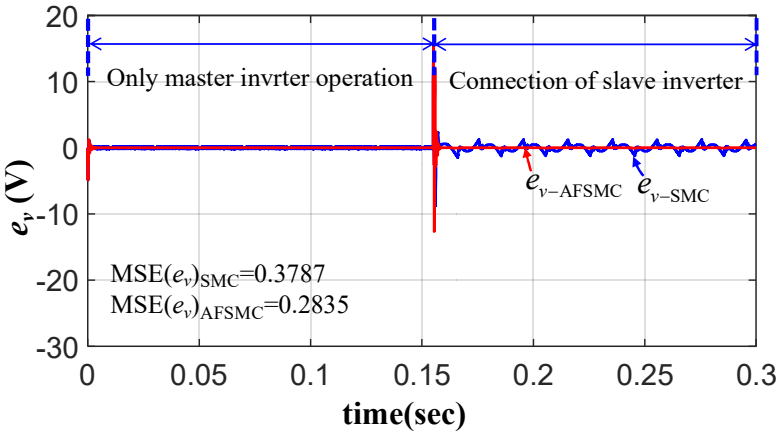

(b)

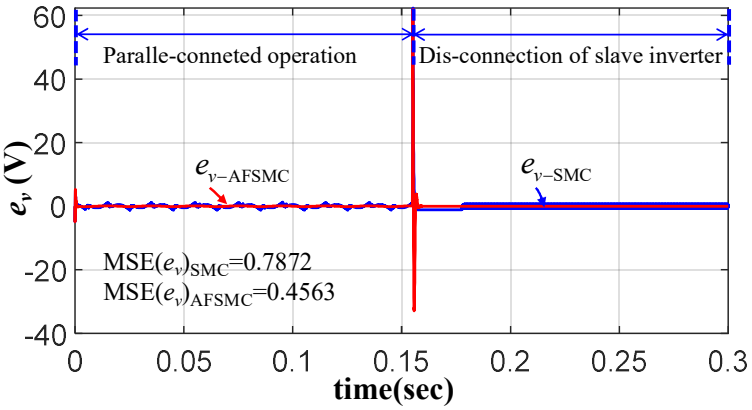

(c)

Figure 8. *Cont.*

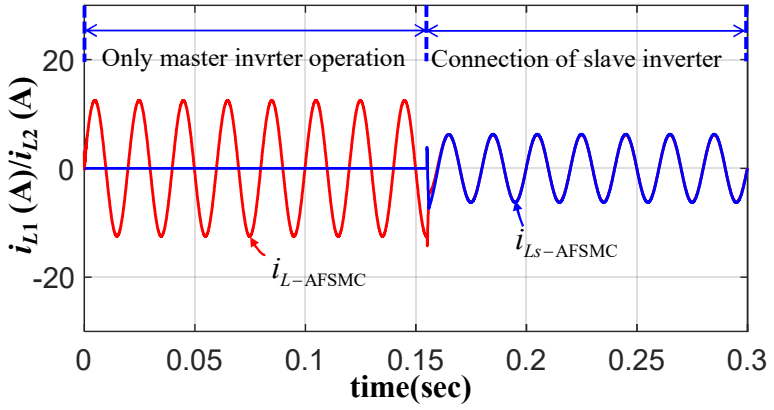

(**d**)

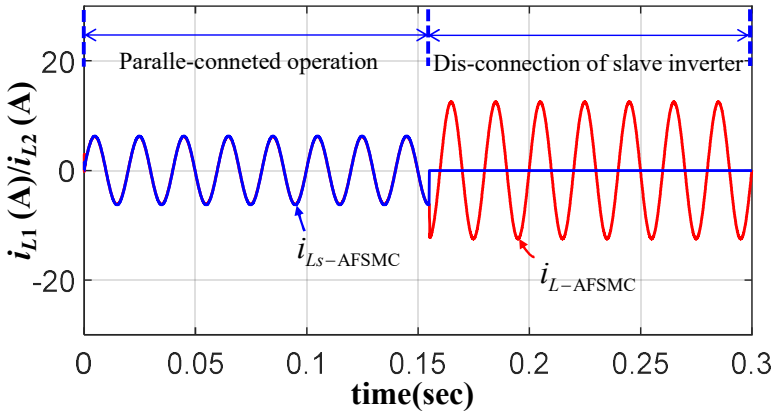

(**e**)

Figure 8. Simulated results of islanded inverter under connection and disconnection of slave inverter: (**a**) output voltage (v_o); (**b**) voltage tracking error under connection; (**c**) voltage tracking error under disconnection; (**d**) Inductor currents (i_L and i_{Ls}) under connection; (**e**) Inductor currents (i_L and i_{Ls}) under disconnection.

The comparison simulation and numerical records between the conventional SMC and the proposed AFSMC scheme under the designed four simulation conditions are implemented in this section, the associated results are shown in Figures 4 and 6–8. One can conclude from the comparisons that the proposed AFSMC scheme significantly improves both the steady state and transient control performance without the chattering phenomenon. Moreover, compared to the increased steady-state errors under the system uncertainties by the SMC framework, the voltage tracking errors can be similar to the errors in the nominal condition by the proposed AFSMC, which demonstrates the effectiveness of the adaptive fuzzy logic system in coping with the system uncertainties and the independence of the accurate mathematical model.

4.2. Experimental Verification

An experimental prototype of the islanded inverter shown in Figure 9 is built up to implement the proposed AFSMC and conventional SMC scheme. In which, the block diagram of the hardware for the prototype and the photograph are depicted in Figure 9a,b, respectively. The corresponding components and the nominal values of the parameters in the designed circuit are described in Table 1.

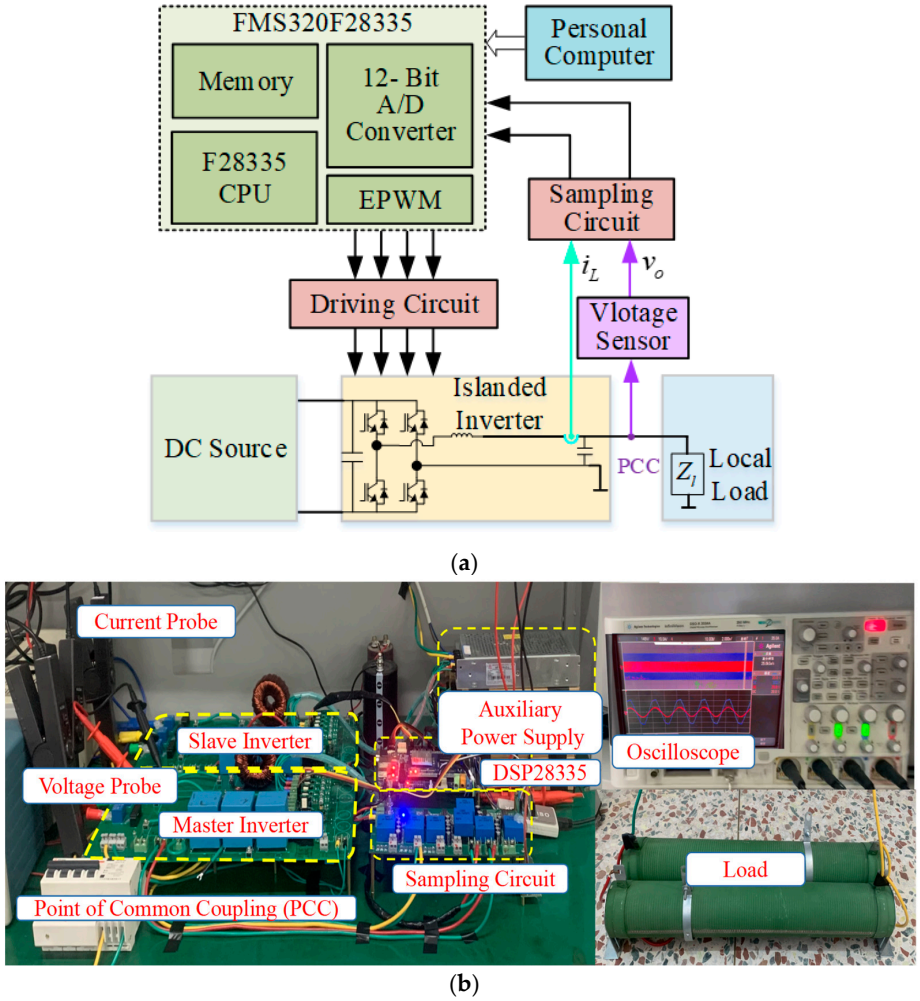

Figure 9. Prototype of islanded inverter: (**a**) Block diagram of hardware; (**b**) Photograph.

The Hall voltage sensors (LV 25-P) and current sensors (LA 55-P) are utilized to measure the output voltage and current signals, respectively. The control systems are carried out on the digital signal processor (DSP) to generate the pulse width modulation (PWM) signals with a sampling frequency of 15 kHz. Then the PWM signals are converted to the gate drive signals of the power switches by the driving circuit based on the TLP250 series IC. The practical experiment is investigated with only a single islanded inverter at the beginning, setting the voltage command as commercial power (220 V@50 Hz), and the current command is generated based (3). Then, the experiment is also implemented under the condition of the slave inverter in current mode connected to the islanded inverter in voltage mode to construct an islanded MG with the master-slave organization to further verify the effectiveness of the proposed AFSMC. Finally, the voltage and current waveforms are displayed on a digital oscilloscope (Agilent DSO-X 3034A).

Figure 10 depicts the experimental results of the single islanded inverter under resistive load by SMC and the proposed AFSMC. One can see that the MSE value of the voltage tracking error is recorded as 0.327 and 0.215, and the total harmonic distortion (THD) valued of the output voltage is 1.83% and 1.15% by the SMC and the proposed FSMC scheme, respectively, which demonstrates that both the two control strategies have good control performance with low MSE and THD in the steady state for the linear resistive load.

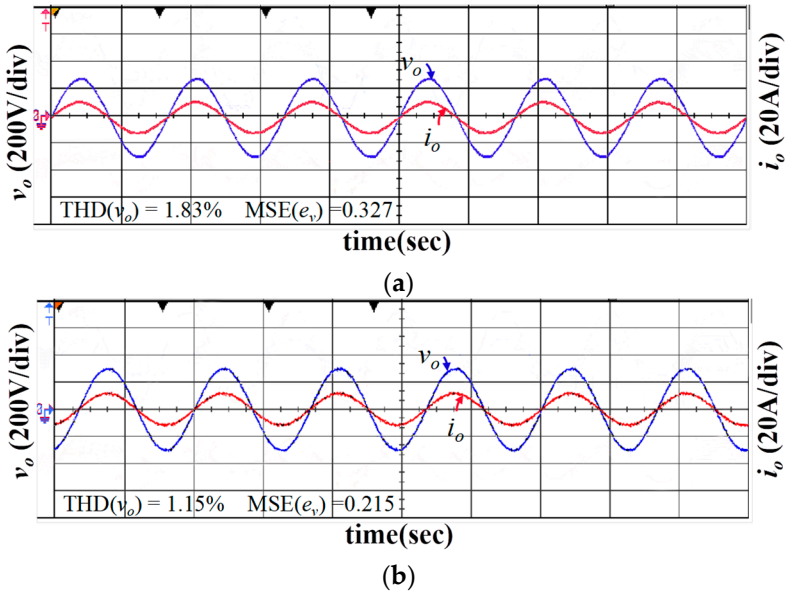

Figure 10. Experimental results under resistive load: (**a**) SMC; (**b**) the proposed AFSMC.

Moreover, the experimental results of the islanded inverter under nonlinear load by the SMC and the proposed AFSMC are shown in Figure 11. The THD and MSE values (2.53% and 0.513) of the SMC in Figure 11a is reduced to 1.45% and 0.305 by the proposed AFSMC in Figure 11b. As can be seen, the islanded inverter system with the proposed AFSMC can supply a higher quality of voltage with lower MSE and THD compared with the inverter with SMC, outputting a slight distortion voltage under the nonlinear rectifier load. This means that the proposed AFSMC scheme has a superior ability to deal with the nonlinear system.

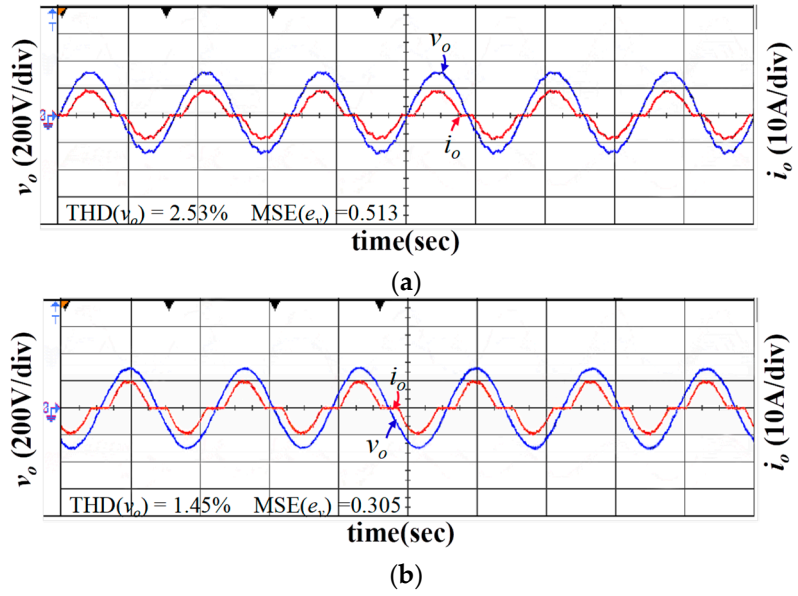

Figure 11. Experimental results under nonlinear load: (**a**) SMC; (**b**) AFSMC.

The experimental results of the islanded inverter under load disturbance with SMC and the proposed AFSMC are shown in Figure 12. As seen in Figure 12, the proposed AFSMC system can significantly reduce the MSE value of voltage tracking error from 0.564 to 0.316 and presents superior robustness against the certainty of load disturbance.

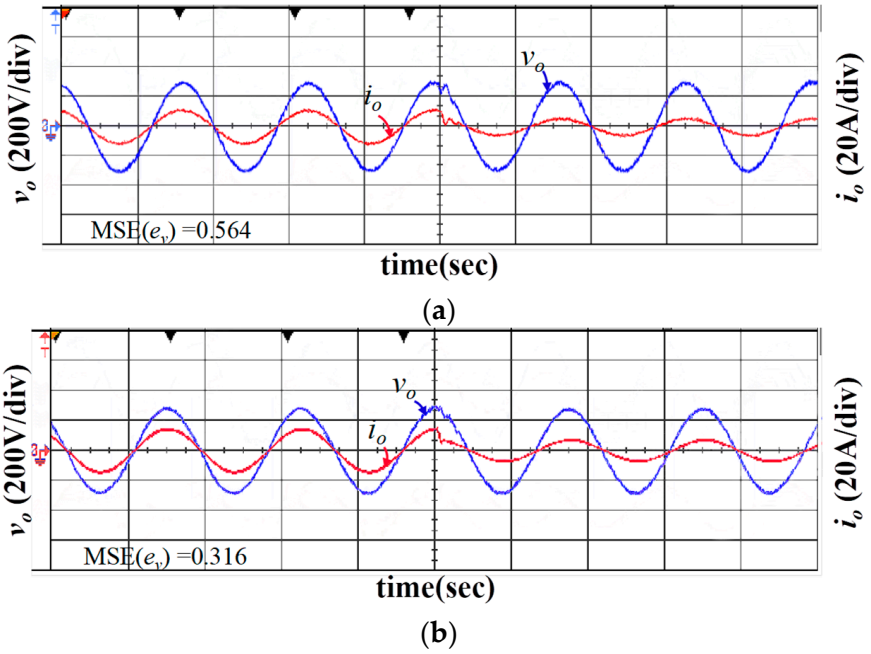

Figure 12. Experimental results under load disturbance: (**a**) SMC; (**b**) proposed AFSMC.

For a practical islanded MG application with the master-slave organization, the interface inverters for DEs are integrated into the point of common coupling (PCC), in which the master inverter works in the voltage mode to supply the stable voltage with its local controller for the MG, and provides the current distribution command for the slave inverters working in the current mode to realize the current/power-sharing with the local current controller. In addition, the slave inverters may be connected to or disconnected from the PCC frequency for troubleshooting. Therefore, the connection and disconnection of the salve inverter is one kind of structure uncertainty for the master inverter in MG.

The experimental results of the islanded inverter under connection and disconnection of the slave inverter are depicted in Figures 13 and 14, respectively. As seen in Figures 13a and 14a, the current of the master inverter is reduced by half due to the current sharing of the connected salve inverter. And the current of the slave inverter is zero after disconnection from the PCC, seen in Figures 13b and 14b, and the remaining master inverter supports the voltage and current to the load standalone. Moreover, there is a chattering phenomenon during the dynamic process in the output voltage under the SMC. Fortunately, the output voltage is less influenced under the model free AFSMC, which significantly ensures the reliability and scalability of the islanded MG.

By comparing the experimental results shown in Figures 10–14, it can be seen that the islanded inverter indeed achieves higher performance by the proposed AFSMC strategy, under the linear resistive or nonlinear load, and even under the occurrence of system uncertainties. The performance comparisons of the SMC and the proposed AFSMC strategy are summarized in Table 2. According to the quantitative analysis, the THD values of the output voltage of the islanded inverter were both constricted inside 1.5% under linear resistive and nonlinear loads by the proposed AFSMC strategy. The proposed AFSMC strategy has improvements in THD of 37.16% and 42.69% and improvements in voltage-tracking MSE values of 34.25% and 40.55% in comparison with conventional SMC under linear resistive and nonlinear loads, respectively. Furthermore, the superior robust voltage tracking performance can be guaranteed even under load disturbance by the proposed AFSMC strategy with 42.12% MSE improvements compared with the conventional SMC scheme. In addition, the proposed AFSMC strategy opposes the ability of parameter self-learning to deal with load disturbance, connection, and disconnection of the slave inverter in micro-grid application without the requirement of a detailed system dynamic. Therefore,

the chattering phenomenon caused by the sign function in the conventional SMC can be remedied effectively, and the control performance and the reliability of the islanded inverter are significantly improved by the proposed AFSMC strategy despite the existence of system uncertainties.

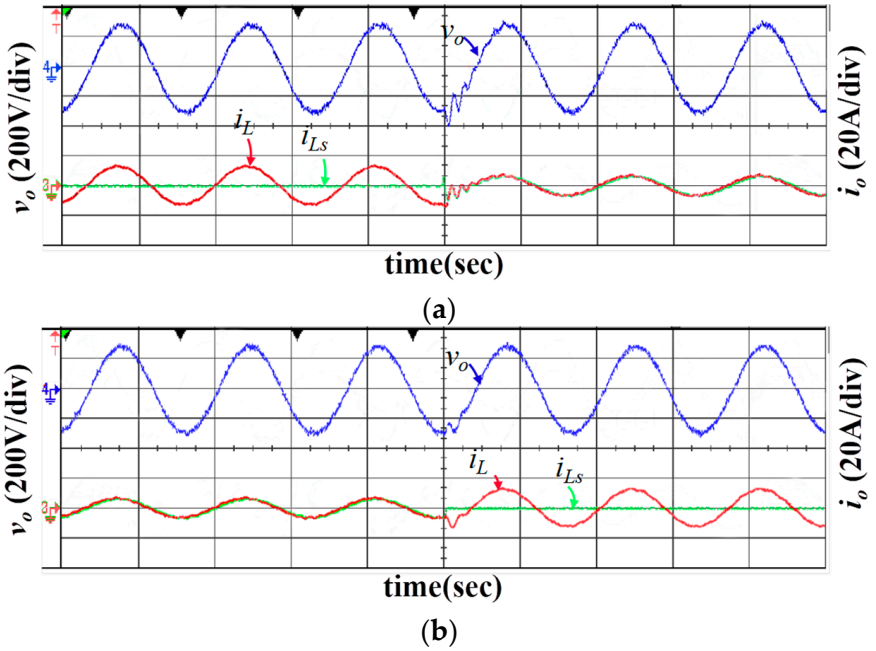

Figure 13. Experimental results under slave inverter connection and disconnection by SMC: (**a**) slave inverter connection; (**b**) slave inverter.

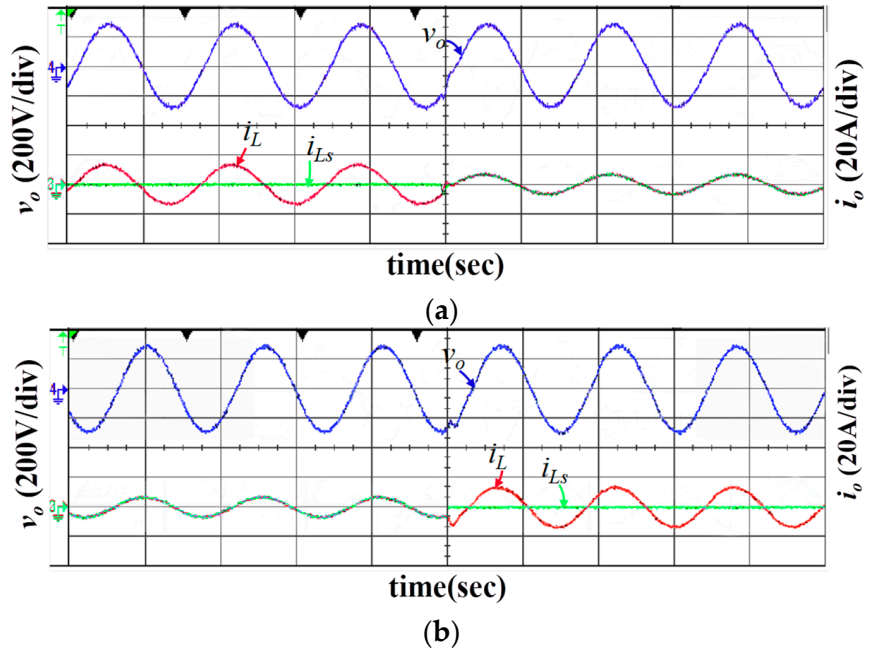

Figure 14. Experimental results under slave inverter connection and disconnection by the proposed AFSMC: (**a**) slave inverter connection; (**b**) slave inverter disconnection.

Table 2. Performance comparisons of SMC and proposed AFSMC.

Performance		SMC	Proposed AFSMC	Improvement Rate
Linear resistive load	THD (v_o)	1.83%	1.15%	37.16%
	MSE (e_v)	0.327	0.215	34.25%
Nonlinear load	THD (v_o)	2.53%	1.45%	42.69%
	MSE (e_v)	0.513	0.305	40.55%
Load disturbance	MSE (e_v)	0.564	0.316	42.12%
	Chattering	Low	None	/
Connection of slave inverter	Chattering	Low	None	/
Disconnection of slave inverter	Chattering	Low	None	/
Learning ability		None	On-line learning	/
Robustness		Good	Favorable	/

5. Conclusions

In order to obtain a high-performance power supply for the islanded inverter, an adaptive fuzzy sliding mode control (AFSMC) strategy is proposed in this paper. The designed total sliding mode surface is adopted as the unique input variable of the fuzzy system, which significantly reduces the number of ruler base. Moreover, in order to remedy the chattering phenomenon, a self-adjustive translation width is introduced to the fuzzy logic system to compensate for the adverse effect of system uncertainties instead of the sign function in conventional SMC law. In addition, to further improve the robustness against the system uncertainties in the islanded inverter, the adaptation algorithm for the translation width and the parameters of the Gaussian membership function are designed by the Lyapunov stability theorem. Thus, both the convergence of the parameters in the fuzzy system and the stability of the proposed AFSMC system can be obtained. Furthermore, the proposed AFSMC and the conventional SMC are implemented in the MATLAB as well as in an experimental prototype. Compared with the conventional SMC, the superior control performance of the proposed AFSMC is demonstrated by the numerical simulation and the experimental results, in which the chattering phenomenon is efficiently eliminated in the output voltage with a low total harmonic distortion (THD) value under various external conditions. Moreover, the proposed model-free AFSMC system has superior robustness with the lower MSE value of the tracking error. In addition, the inverter system with the proposed AFSMC has the flexible scalability of allowing the slave inverters to connect or disconnect without powering off in the islanded MG with the master-slave organization.

The investigation of the proposed AFSMC scheme with satisfactory robust performance for the islanded inverter in this study has great value for guaranteeing stability and providing strong support to the islanded MG with the master-slave organization. Moreover, the proposed AFSMC, as a model-free alternative methodology, has a general use. It can manifest the giant value to handle system uncertainty and nonlinearity, and can release the dependence on accurate dynamic models of the control plant. Therefore, except for the islanded inverter, the proposed AFSMC with a simple control structure and inference mechanism has great potential to be extended to power electronic converter control, motor control, manipulator control, and other various practical applications.

Author Contributions: Mathematical modeling, methodology, Y.Y., Y.W. and R.L.; hardware, Y.Y. and W.Z.; software, Z.L. and W.Z.; validation, Z.L. and W.Z.; writing—original draft preparation, Y.Y.; writing—review and editing Y.W., Y.Y. and R.L. All authors are involved in improving the overall contents of the manuscript. All authors have read and agreed to the published version of the manuscript.

Funding: This research was funded by the Natural Science Research Project of Huaian (HAB201905); Huai'an key laboratory of motion control and converter technology under Grant (HAP201903); Natural Science Research Project of Huaian (HAB202062).

Conflicts of Interest: The authors declare no conflict of interest.

References

1. Venkatramanan, D.; John, V. A Reconfigurable Solar Photovoltaic Grid-Tied Inverter Architecture for Enhanced Energy Access in Backup Power Applications. *IEEE Trans. Ind. Electron.* **2020**, *67*, 10531–10541. [CrossRef]
2. Yazdani, S.; Ferdowsi, M.; Davari, M.; Shamsi, P. Advanced Current-Limiting and Power-Sharing Control in a PV-Based Grid-Forming Inverter Under Unbalanced Grid Conditions. *IEEE J. Emerg. Sel. Top. Power Electron.* **2020**, *8*, 1084–1096. [CrossRef]
3. Alzahrani, A.; Ramu, S.K.; Devarajan, G.; Vairavasundaram, I.; Vairavasundaram, S. A Review on Hydrogen-Based Hybrid Microgrid System: Topologies for Hydrogen Energy Storage, Integration, and Energy Management with Solar and Wind Energy. *Energies* **2022**, *15*, 7979. [CrossRef]
4. Vasantharaj, S.; Indragandhi, V.; Subramaniyaswamy, V.; Teekaraman, Y.; Kuppusamy, R.; Nikolovski, S. Efficient Control of DC Microgrid with Hybrid PV—Fuel Cell and Energy Storage Systems. *Energies* **2021**, *14*, 3234. [CrossRef]
5. Kakran, S.; Chanana, S. Smart operations of smart grids integrated with distributed generation: A review. *Renew. Sust. Energ. Rev.* **2018**, *81*, 524–535. [CrossRef]
6. Li, D.; Man Ho, C.N. A Delay-Tolerable Master–Slave Current-Sharing Control Scheme for Parallel-Operated Interfacing Inverters with Low-Bandwidth Communication. *IEEE Trans. Ind. Appl.* **2020**, *56*, 1575–1586. [CrossRef]
7. Rahmani, S.; Rezaei-Zare, A.; Rezaei-Zare, M.; Hooshyar, A. Voltage and Frequency Recovery in an Islanded Inverter-Based Microgrid Considering Load Type and Power Factor. *IEEE Trans. Smart Grid.* **2019**, *10*, 6237–6247. [CrossRef]
8. Sadek, S.M.; Omran, W.A.; Hassan, M.A.M.; Talaat, H.E.A. Data Driven Stochastic Energy Management for Isolated Microgrids Based on Generative Adversarial Networks Considering Reactive Power Capabilities of Distributed Energy Resources and Reactive Power Costs. *IEEE Access* **2021**, *9*, 5397–5411. [CrossRef]
9. Sahoo, A.K.; Mahmud, K.; Crittenden, M.; Ravishankar, J.; Padmanaban, S.; Blaabjerg, F. Communication-Less Primary and Secondary Control in Inverter-Interfaced AC Microgrid: An Overview. *IEEE J. Emerg. Sel. Top. Power Electron.* **2020**, *9*, 5164–5182. [CrossRef]
10. El-Sayed, W.T.; Azzouz, M.A.; Zeineldin, H.H.; El-Saadany, E.F. A Harmonic Time-Current-Voltage Directional Relay for Optimal Protection Coordination of Inverter-Based Islanded Microgrids. *IEEE Trans. Smart Grid.* **2021**, *12*, 1904–1917. [CrossRef]
11. Yang, Y.; Wai, R.J. Design of Adaptive Fuzzy-Neural-Network-Imitating sliding-mode Control for Parallel-Inverter System in Islanded Micro-grid. *IEEE Access* **2021**, *9*, 56376–56396. [CrossRef]
12. Dehghani, M.; Niknam, T.; Ghiasi, M.; Baghaee, H.R.; Blaabjerg, F.; Dragicevŭć, T.; Rashidi, M. Adaptive backstepping control for master-slave AC microgrid in smart island. *Energy* **2022**, *246*, 123282. [CrossRef]
13. Saxena, A.; Chauhan, D.S. Simulation and Comparative Analysis of Single-phase H Bridge Micro Inverters with Conventional PI Control and Virtual Output Impedance Control: A Case Study. *Int. J. Power Electron.* **2021**, *14*, 336–365. [CrossRef]
14. Selvaraj, J.; Rahim, N.A. Multilevel Inverter for Grid-Connected PV System Employing Digital PI Controller. *IEEE Trans. Ind. Electron.* **2009**, *56*, 149–158. [CrossRef]
15. Jiang, X.; He, C.; Jermsittiparsert, K. Online Optimal Stationary Reference Frame Controller for Inverter Interfaced Distributed Generation in A Microgrid System. *Energy Rep.* **2020**, *6*, 134–145. [CrossRef]
16. Nguyen, T.H.; Kim, K.H. Finite Control Set–model Predictive Control with Modulation to Mitigate Harmonic Component in Output Current for A Grid-connected Inverter under Distorted Grid Conditions. *Energies* **2017**, *10*, 907. [CrossRef]
17. Mestriner, D.; Rosini, A.; Xhani, I.; Bonfiglio, A.; Procopio, R. Primary Voltage and Frequency Regulation in Inverter Based Islanded Microgrids through a Model Predictive Control Approach. *Energies* **2022**, *15*, 5077. [CrossRef]
18. Young, H.A.; Marin, V.A.; Pesce, C.; Rodriguez, J. Simple Finite-Control-Set Model Predictive Control of Grid-forming Inverters with LCL Filters. *IEEE Access* **2020**, *8*, 81246–81256. [CrossRef]
19. Azab, M. A Finite Control Set Model Predictive Control Scheme for Single-phase Grid-connected Inverters. *Renew. Sustain. Energy Rev.* **2021**, *135*, 110131. [CrossRef]
20. Yin, Z.; Hu, C.; Luo, K.; Rui, T.; Feng, Z.; Lu, G.; Zhang, P. A Novel Model-Free Predictive Control for T-Type Three-Level Grid-Tied Inverters. *Energies* **2022**, *15*, 6557. [CrossRef]
21. Zhang, Z.; Li, B.; Ma, R.; Chen, X.; Dai, Z. Finite-Control-Cet Model Predictive Control with A Constant Switching Frequency for Single-phase Grid-connected Photovoltaic Inverter. *IET Power Electron.* **2022**, *15*, 123–131. [CrossRef]
22. Chen, T.; Abdel-Rahim, O.; Peng, F.; Wang, H.W. An Improved Finite Control Set-MPC-Based Power Sharing Control Strategy for Islanded AC Microgrids. *IEEE Access* **2020**, *8*, 52676–52686. [CrossRef]
23. Estrada, L.; Vazquez, N.; Vaquero, J.; Hernandez, C.; Arau, J.; Huerta, H. Finite Control Set–Model Predictive Control Based On Sliding Mode For Bidirectional Power Inverter. *IEEE Trans. Energy Convers* **2021**, *36*, 2814–2824. [CrossRef]
24. Yang, H.; Zhang, Y.; Liang, J.; Gao, J.; Walker, P.D.; Zhang, N. Sliding-modesliding-mode observer based voltage-sensorless model predictive power control of PWM rectifier under unbalanced grid conditions. *IEEE Trans. Ind. Electr.* **2017**, *65*, 5550–5560. [CrossRef]
25. Liang, Y.; He, Y.; Niu, Y. Robust Errorless-Control-Targeted Technique Based on MPC for Microgrid with Uncertain Electric Vehicle Energy Storage Systems. *Energies* **2022**, *15*, 1398. [CrossRef]
26. Liu, Z.F.; DU, G.P.; DU F., D. Research Status and Development Trend of Finite Control Set Model Predictive Control in Power Electronics, Trans. *China Electrothchenical Soc.* **2017**, *32*, 58–69.
27. Novak, M.; Nyman, U.M.; Dragicevic, T.; Blaabjerg, F. Analytical Design and Performance Validation of Finite Set MPC Regulated Power Converters. *IEEE Trans. Ind. Electron.* **2019**, *66*, 2004–2014. [CrossRef]

28. Wang, F.; Davari, S.A.; Chen, Z.; Zhang, Z.; Khaburi, D.A.; Rodrieguez, J.; Kennel, R. Finite control set model predictive torque control of induction machine with a robust adaptive observer. *IEEE Trans. Ind. Electron.* **2016**, *64*, 2631–2641. [CrossRef]
29. Zhang, Y.; Yin, Z.; Li, W.; Liu, J. Adaptive sliding-mode-based Speed Control in Finite Control Set Model Predictive Torque Control for Induction Motors. *IEEE Trans. Ind. Electron.* **2020**, *36*, 8076–8087. [CrossRef]
30. Cortes, D.; Vazquez, N.; Alvarez-Gallegos, J. Dynamical Sliding-Mode Control of the Boost Inverter. *IEEE Trans. Ind. Electron.* **2009**, *56*, 3467–3476. [CrossRef]
31. Rafiq, M.A.; Ulasyar, A.; Uddin, W.; Zad, H.S.; Khattak, A.; Zeb, K. Design and Control of a Quasi-Z Source Multilevel Inverter Using a New Reaching Law-Based Sliding Mode Control. *Energies* **2022**, *15*, 8002. [CrossRef]
32. Delghavi, M.B.; Yazdani, A. sliding-mode Control of AC Voltages and Currents of Dispatchable Distributed Energy Resources in Master-Slave-Organized Inverter-Based Microgrids. *IEEE Trans. Smart Grid* **2019**, *10*, 980–991. [CrossRef]
33. Chang, F.-J.; Chang, E.-C.; Liang, T.-J.; Chen, J.-F. Digital-signal-processor-based DC/AC inverter with integral-compensation terminal sliding-mode control. *IET Power Electron.* **2011**, *4*, 159–167. [CrossRef]
34. Chen, Z.; Luo, A.; Wang, H.; Chen, Y.; Li, M.; Huang, Y. Adaptive sliding-mode voltage control for inverter operating in islanded mode in microgrid. *Int. J. Elec. Power.* **2015**, *66*, 133–143. [CrossRef]
35. Baghaee, H.R.; Mirsalim, M.; Gharehpetian, G.B.; Talebi, H.A. A Decentralized Power Management and Sliding Mode Control Strategy for Hybrid AC/DC Microgrids including Renewable Energy Resources. *IEEE Trans. Ind. Informat.* **2017**, *3*. [CrossRef]
36. Al Sumarmad, K.A.; Sulaiman, N.; Wahab, N.I.A.; Hizam, H. Energy Management and Voltage Control in Microgrids Using Artificial Neural Networks, PID, and Fuzzy Logic Controllers. *Energies* **2022**, *15*, 303. [CrossRef]
37. Annapoorani, K.I.; Rajaguru, V.; Padmanabhan, S.A.; Kumar, K.M.; Venkatachalam, S. Fuzzy logic-based integral controller for load frequency control in an isolated micro-grid with superconducting magnetic energy storage unit. *Mater. Today Proc.* **2022**, *58*, 244–250. [CrossRef]
38. Rao, S.N.V.B.; Kumar, Y.V.P.; Pradeep, D.J.; Reddy, C.P.; Flah, A.; Kraiem, H.; Al-Asad, J.F. Power Quality Improvement in Renewable-Energy-Based Microgrid Clusters Using Fuzzy Space Vector PWM Controlled Inverter. *Sustainability* **2022**, *14*, 4663. [CrossRef]
39. Wai, R.J.; Su, K.H. Adaptive enhanced fuzzy sliding-mode control for electrical servo drive. *IEEE Trans. Ind. Electron.* **2006**, *53*, 569–580.
40. Lin, J.; Zou, T.; Zhang, F.; Zhang, Y. Yaw Stability Research of the Distributed Drive Electric Bus by Adaptive Fuzzy Sliding Mode Control. *Energies* **2022**, *15*, 1280. [CrossRef]
41. Khanesar, M.A.; Branson, D. Robust Sliding Mode Fuzzy Control of Industrial Robots Using an Extended Kalman Filter Inverse Kinematic Solver. *Energies* **2022**, *15*, 1876. [CrossRef]
42. Zhu, Y.; Fei, J. Disturbance Observer Based Fuzzy Sliding Mode Control of PV Grid Connected Inverter. *IEEE Access* **2018**, *6*, 21202–21211. [CrossRef]
43. Hou, S.; Fei, J.; Chu, Y.; Chen, C. Experimental Investigation of Adaptive Fuzzy Global Sliding Mode Control of Single-Phase Shunt Active Power Filters. *IEEE Access* **2019**, *7*, 64442–64449. [CrossRef]
44. Fang, Y.; Fei, J.; Wang, T. Adaptive Backstepping Fuzzy Neural Controller Based on Fuzzy Sliding Mode of Active Power Filter. *IEEE Access* **2020**, *8*, 96027–96035. [CrossRef]
45. Astrom, K.J.; Wittenmark, B. *Adaptive Control*; Addison-Wesley: New York, NY, USA, 1995.